Redox Controls during Magma Ocean Degassing

Fabrice Gaillard, Fabien Bernadou, Mathieu Roskosz, Mohamed Ali Bouhifd, Yves Marrocchi, Giada Iacono-Marziano, Manuel Moreira, Bruno Scaillet, Gregory Rogerie

Redox Controls during Magma Ocean Degassing

Fabrice Gaillard[1], Fabien Bernadou[1], Mathieu Roskosz[2], Mohamed Ali Bouhifd[3], Yves Marrocchi[4], Giada Iacono-Marziano[1], Manuel Moreira[1], Bruno Scaillet[1], Gregory Rogerie[1].

[1] : Institut des Sciences de la Terre d'Orléans, CNRS/Université d'Orléans/BRGM, 1a rue de la Férollerie 45071, Orléans cedex 2, France
[2] : IMPMC, MNHN, CNRS, UMR 7590, Muséum National d'Histoire Naturelle, Sorbonne Universités, CP 52, 57 rue Cuvier, Paris F-75231, France.
[3] : Laboratoire Magmas et Volcans, Université Clermont Auvergne, CNRS, IRD, OPGC, F-63000 Clermont-Ferrand, France.
[4] : Université de Lorraine, CNRS, CRPG, F-54000 Nancy, France

Nitrogen, carbon, hydrogen and sulfur are essential elements for life and comprise about 1 % of terrestrial planet masses. These elements dominate planetary surfaces due to their volatile nature, but the Earth's interior also constitutes a major C-H-N-S reservoir. Resolving the origin of the surficial versus deep volatile reservoirs requires the past 4.5 Giga-years of mantle outgassing and ingassing processes to be reconstructed, involving many unknowns. As an alternative, we propose to define the primordial distribution of volatiles resulting from degassing of the Earth's magma ocean (MO). The equilibrium partitioning of C-H-O-N-S elements between the MO and its atmosphere is calculated by means of solubility laws, extrapolated to high temperatures and over a large range of redox conditions. Depending on the redox conditions, the amount of volatiles, and the size of the MO considered, we show that the last MO episode may have degassed 40-220 bar atmospheres, whereas hundreds to thousands of ppm of C-H-O-N-S can be retained in the magma. Two contrasting scenarios are investigated: reduced vs. oxidized MO. For reduced cases (<IW-2), an H-C±N-rich atmosphere can be formed, whereas the atmosphere under oxidizing conditions (>IW+2) would be dry and C-N-S-rich. An intermediate redox state produces a C-N atmosphere. In many cases, the present-day surficial abundances (atmosphere+ocean+crust) of C and N, the most volatile elements, are very close to the calculated primordial MO - atmosphere distribution. This probably means that lithospheric recycling and post-magma ocean degassing only moderately alter the surficial abundances of these elements. Sulfur, in contrast, must have been mostly outgassed by post-MO events. Changes in redox conditions during magma ocean degassing played a first order role in the composition of the primordial atmosphere of planets. We suggest that the more oxidized conditions on Venus due to H-loss may have played a role in the growth of a dry MO atmosphere on this planet compared to an H-bearing one on Earth. To verify these first order assertions, constraints on volatile behaviour under extreme magma ocean conditions and upon magma ocean solidification are urgently needed.

1. Introduction

The life-forming elements (carbon, hydrogen, oxygen, nitrogen and sulfur; hereafter CHONS) are abundant on the Earth's surface and dominate most surficial biogeochemical cycles. However, it is known that the planetary interior represents at least an equivalent CHONS reservoir (Marty et al., 2020; Hirschmann, 2018; Gaillard et al., 2021). Two CHONS mantle reservoirs have been identified: (i) depleted mantle (DM), corresponding to the source of mid-ocean ridge magmatism (Hirschmann and Dasgupta, 2009; Saal et al., 2002; LeVoyer et al., 2017), and (ii) deep enriched mantle (EM) reservoirs, fueling most hotspots (Hofmann, 2003; Hirschmann and Dasgupta, 2009; Marty et al, 2020; Miller et al., 2019). Historically, these reservoirs have not been defined in terms of volatile CHONS components, but on various trace element and isotope ratios that are linked to the formation of the crust (Hofmann, 2003). Their definition in terms of volatile reservoirs is therefore a work in progress. Difficulties arise partly from the fact that these two reservoirs are not homogeneous, making their definition and their CHONS contents highly debated. Their respective volumes are also poorly known. The volume of the depleted mantle (DM) is at least equivalent to that of the upper mantle and may extend down to a region just above the core – mantle boundary (Hoffman, 2003; Miller et al., 2019), where puzzling geophysical discontinuities possibly delineate deep geochemical reservoirs. The deep EM contains primordial material with unusual Sun-like He, Ne and N isotopic compositions that are significantly distinct from those of the DM (Marty et al., 2016, 2020; Tucker and Mukopadhay, 2014). The EM is enriched with respect to the DM in both carbon and hydrogen but the magnitude of this enrichment remains unclear (e.g. Miller et al., 2019 vs. Hirschmann 2018 for C, and Marty et al., 2020 vs. Hirschmann, 2018 for H).

The origin and evolution of the distribution of the CHONS elements between the depleted and enriched mantles and how they connect to CHONS abundances at the Earth' surface is also a matter of lively debate. The deep enriched mantle may have been isolated for a long time from the mantle convection sourcing mid-ocean-ridge magma (linked to plate tectonics, e.g. Ballmer et al., 2017; Tucker and Mukhopdhay 2014). However, mantle plumes, mantle degassing and lithospheric recycling (i.e. ingassing) have been operating for a long time and potentially caused extensive redistribution of CHONS between mantle and surface reservoirs (Hirschmann and Dasgupta, 2009; Sleep, 2011; Hirschmann, 2018). There is, however, no consensus on the CHONS reservoirs and fluxes associated with subduction processes and mantle outgassing. For example, published estimations of the present-day amount of subducted carbon range from 0 to 52 Mt C / years (Kelemen and Manning, 2016). All these uncertainties mean that the estimation

of the primordial distribution of volatile elements, as well as their evolution within the different reservoirs, remains highly hypothetical (Hirschmann, 2018).

As an alternative approach to this question, we propose to reconstruct the primordial volatile distributions inherited from planetary accretion and early differentiation stages making up the Hadean. Although no rock specimens have survived from the Hadean eon, some zircon crystals indicate that an early atmosphere, crust, oceans, and possibly life, were most likely established within the first 100 million years of the Earth's history (Catling and Zahnle, 2020). Consistent with such an early evolution, geochemical surveys indicate that most of the CHONS elements were delivered during accretion (Marty et al., 2016; Sarafian et al., 2014; Greenwood et al., 2018; Piani et al., 2020) and were thus processed by the various differentiation events, in particular the magma ocean stages (Pahlevan et al, 2019; Grewal et al., 2020; Sossi et al., 2020) (see Fig. 1). In this context, even if a significant late veneer has contributed to refining the final volatile reservoirs of the Earth, its contribution would not be greater than 10% (Marty et al., 2013), which would not alter the conclusion that volatiles were efficiently processed during the early magma ocean stages. Here, we present a model that predicts CHONS partitioning between magma and gas in the context of magma ocean – atmosphere interaction. We show that oxygen fugacity is the key parameter ruling such partitioning. We found that for N and C, i.e. the most volatile elements, the magma ocean outgassed a mass similar to the present-day surficial reservoirs. Hydrogen can only be degassed under reduced conditions, whereas sulfur is only volatile in conditions as oxidized as the present-day mantle. This pushes back the prerequisite conditions for life to the early stages of planetary systems.

2. Conditions of MO degassing.

2.1. General framework and assumptions

Magma oceans (MO) experienced extreme thermodynamic conditions: high temperature, low viscosity, and vigorous convection enabled efficient mass transfer and large-scale chemical equilibration during planetary differentiation (Fig. 1) (eg. Elkins-Tanton, 2012; Rubie et al., 2015). Gas-melt equilibration certainly occurred at the MO – atmosphere interface (Lebrun et al., 2013; Hamano et al., 2013; Sossi et al., 2020; Katyal et al., 2020). The equilibrium CHONS partitioning was thus governed by speciation in both the melt and gas, which was in turn controlled by the pressure (P), temperature (T) and oxygen fugacity (fO_2) conditions prevailing at this interface. This simplification holds as long as convection in both the MO and its overlying atmosphere is fast enough. However, fast convection also implies rapid cooling,

which would have caused rapid crystallization of the MO (ie. Elkins-Tanton, 2012 ; Lebrun et al., 2013 ; Hamano et al., 2013 ; Rubie et al., 2015 ; Hier-Majumder and Hirschmann, 2017). In this respect, most simulations suggest that the cooling and solidification of the Earth's last MO occurred rapidly, within less than ca. 4-5 millions of years (Myrs) (Hamano et al., 2013). Alternatively, degassing and greenhouse effects may extend the lifetime of a MO to several tens of millions of years, but in any case, crystallization must have been relatively fast. Two end-member cases can be identified: (a) crystallization is so rapid that the molten MO – atmosphere partitioning is preserved, and (b) CHONS volatiles can be segregated during crystallization of the MO (eg. Hier-Majumder and Hirschmann, 2017) producing deep volatile reservoirs. The possibility of deep segregation of volatiles is not explored in this study. We will mainly discuss situation (a), where gas – melt equilibria are controlled by the prevailing P-T-fO_2 at the MO – atmosphere interface.

The temperature is set at T=1500°C, which is low when considering MO conditions (Sossi et al., 2020). Such a temperature avoids an unreasonable extrapolation of COHNS solubility laws that have been defined at <1300°C (see Supplementary methods, Iacono-Marziano et al., 2012; Bernadou et al., 2021). For the sake of completeness, tests up to T=1920°C (fig. S1) were carried out. It shows a weak model sensitivity at this temperature. It would be good to carry out accurate calibrations of speciation and solubility laws during melt - gas equilibria at ~2000°C in the future.

Pressure is defined by the weight of the atmosphere applied at the surface of the MO as explained below. Finally, oxygen fugacity is treated as a variable input parameter.

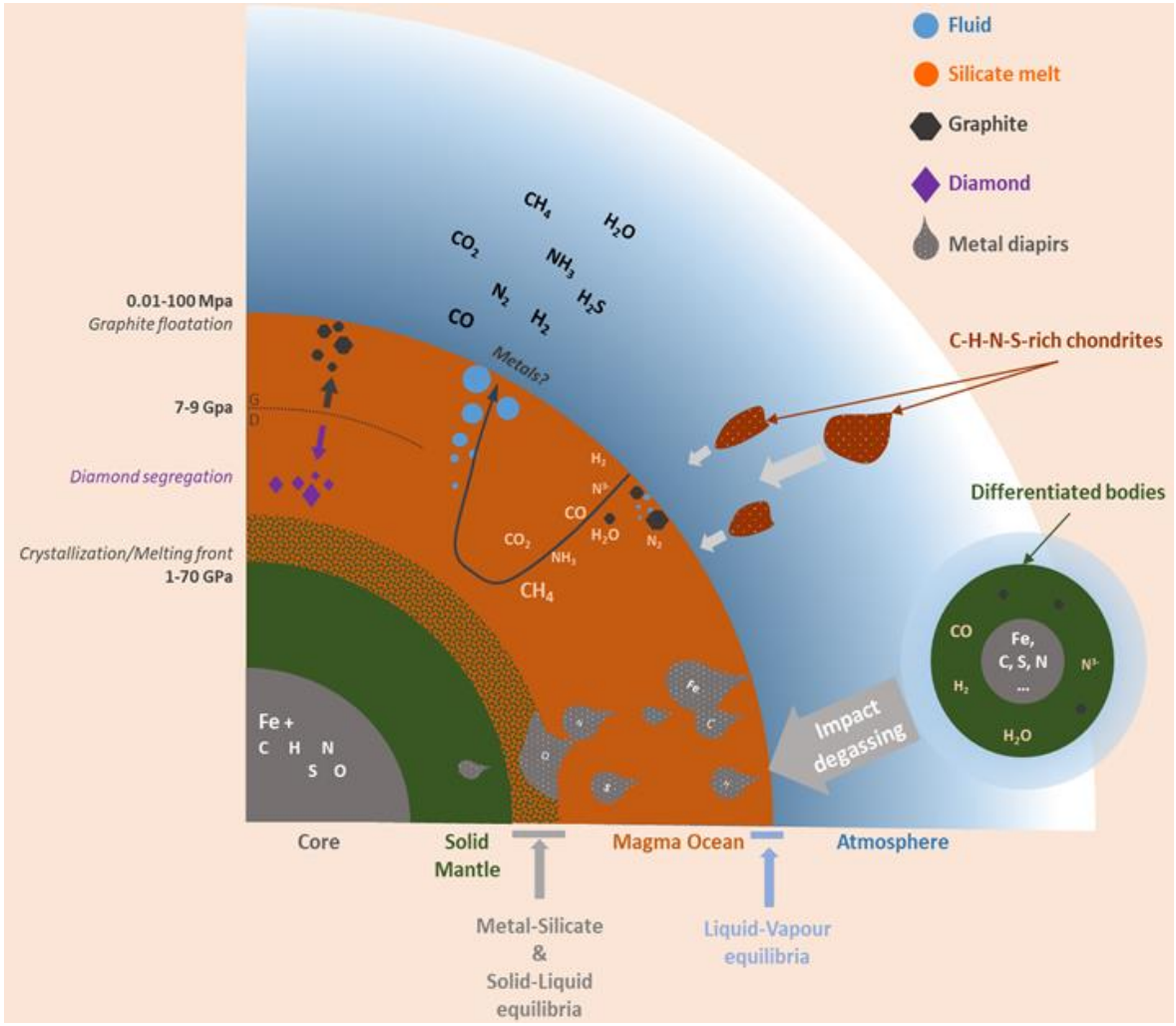

Figure 1. The early fate of C-H-O-N-S elements in a MO. Life-essential elements are processed through a three-body problem involving the core, the silicate MO and the atmosphere. The delivery of C-H-O-N-S elements is carried out via accretion of both chondritic material and differentiated small bodies. The incorporated C-H-O-N-S elements partition between the convective silicate MO, the sinking metal diapirs, and the rising fluids (bubbles). A variety of species can dissolve in the MO and the atmosphere. In addition, under the typically reducing conditions of the MO, graphite (G) and/or diamond (D) saturation in the MO can store a significant part of the carbon that is present in the system. These carbon phases respectively float to the surface and sink to a depth in the MO, thus indirectly impacting the MO outgassing dynamics. This study uses gas – silicate melt equilibria to predict the MO–atmosphere exchanges. The pressure at the MO – atmosphere interface is controlled by the weight of the atmosphere, which is determined by the mass of the MO atmosphere.

Mantle depletion in different siderophile elements suggests that strongly reducing conditions prevailed during the early differentiation of the Earth, i.e. IW-5, before they turned more oxidizing during the final stages of core formation, i.e. IW-2 (Wade and Wood, 2005; Rubie et al., 2015). This is deduced from metal-silicate equilibria taking place at the base of the MO (Fig.1). However, the actual redox state that prevailed at the MO surface, where degassing took

place (Fig. 1), is still under debate (eg. Pahlevan et al., 2019; Armstrong et al., 2019; Keppler and Gobalek, 2019; Sossi et al., 2020):

(i) On the one hand, Armstrong et al. (2019) reports the enhanced stability of ferric iron in silicate melts at elevated pressure (ie. >10 GPa). This implies that if metal – silicate equilibrium buffers the fO_2 at great depth in the MO (>500 km), a surficial MO with f_{O2} conditions similar to that of the present-day mantle (i.e. close to the FMQ buffer) must have prevailed. This suggests that the MO ferric iron content was in the range 3-10% relative iron (Fe^{3+}/Fe_{tot} =0.03-0.1). Such an oxidized MO would be broadly consistent with conditions required to prevent hydrogen escape (Pahlevan et al., 2019).

(ii) On the other hand, Keppler and Gobalek (2019) suggest that graphite flotation may have prevailed during most of the MO stage. If true, the fO_2 conditions prevailing in the shallow mantle were not necessarily buffered by ferric-ferrous equilibria. The combination of graphite buoyancy and the particular f_{O2}-depth relationships of the C-CO equilibria, may have imposed f_{O2} conditions in the shallow MO as low as IW-5 (Fig. 2., Shirayev and Gaillard, 2014). In fact, the prevailing fO_2 would be inversely proportional to the pressure at the MO – atmosphere interface (Shirayev and Gaillard, 2014). Whether such low fO_2 would cause massive H_2 escape remains uncertain since the predicted timescales of both H-escape and cooling of a MO in putative H_2-rich atmosphere are of similar orders (ie. Katyal et al., 2020). These rates should, in addition, be controlled by the ratio of H dissolved in the MO vs. H outgassed into the atmosphere, which is not considered in models of atmospheric escape.

(iii) In between, Sossi et al. (2020) use the present-day mantle ferric-ferrous iron fraction in the solid upper mantle (Fe^{3+}/Fe_{tot} ~ 0.04) to propose an MO at an fO_2 of ca. IW+0.5±0.7. This MO model does not assume any particular prevailing redox mechanism, but takes the present-day mantle oxidation state as being representative of the MO.

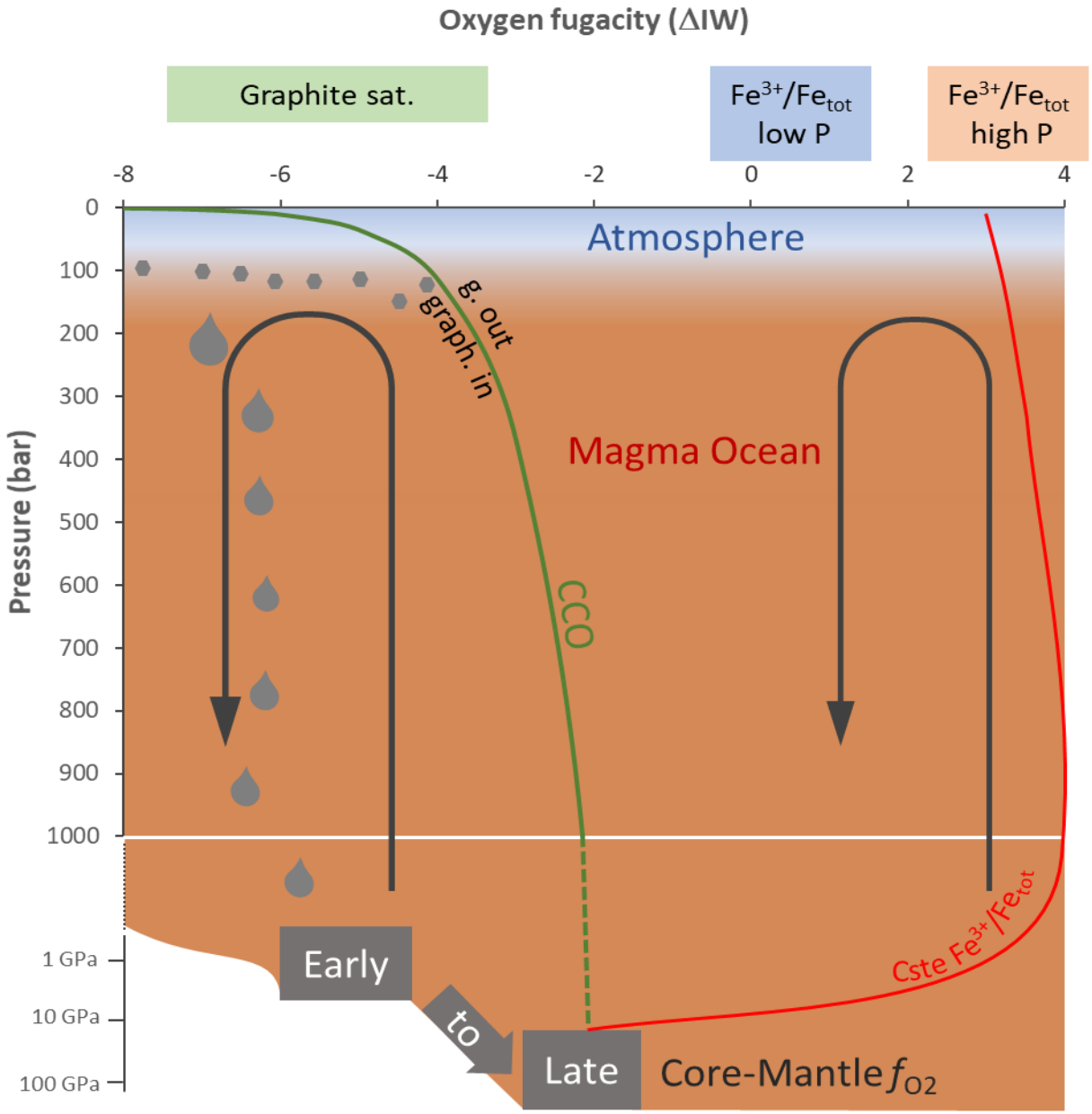

Figure 2. The range of fO_2 conditions prevailing in the basal and surficial MO. The three top-boxes illustrate the three cases discussed in the text, from high to low fO_2: Armstrong et al (2019) propose high fO_2 conditions in the surficial MO based on high pressure disproportionation reactions involving iron, Sossi et al (2020) propose a moderately reduced MO based on low pressure ferric-ferrous equilibria, and finally, assuming graphite floatation (Keppler and Gobalek, 2019), we consider the most reduced case when the CCO buffer prevails at low pressure. At low pressure, the CCO buffer can be as reduced as IW-5 (calculation done at 1750°C). One can nevertheless see that, at high pressure, the fO_2 of the CCO buffer can be reconciled with that of metal-silicate equilibration implying that graphite saturation imposes very low fO_2 at the surface of the MO, while the mantle body itself can remain more oxidized.

These contrasting views require f_{O2} to be considered as a variable in our model of MO degassing. State of the art models for MOs simultaneously calculate crystallization and degassing, but are limited to CO_2-H_2O atmospheres (eg. Elkins-Tanton, 2012; Le Brun et al., 2013; Hamano et al., 2013), implicitly restricting models to a 2-volatile component system and assuming that the redox conditions in the surficial MO were similar to the present-day mantle. Addressing the multi-component nature and the variation in oxidation state of species in the CHONS system is an important step towards addressing the diversity of possible conditions prevailing in early MOs. Here, we deploy a model where graphite and C-H-O-N-S species dissolved in the MO depend on the partial pressure and mass of coexisting gas species, including oxygen (O_2, see section 3).

2.2. Volatile contents as a function of the MO size

The aim of this study is to quantify the volatile budgets formed during the last magma – atmosphere equilibration stages. For this purpose, a summary of the mass and size of these surficial and deep volatile reservoirs is available in Table 1, together with the four types of simulated runs. An Earth-sized planet is considered, and results for variable MO masses (from 1/4 to the full bulk silicate Earth (BSE)) are shown. The surficial volatile inventory, (i.e. atmosphere + ocean + crust, after Marty, 2012; Hirschmann, 2018) was systematically considered in our calculations. We added to this surficial CHNS inventory the volatiles in various mantle reservoirs: Case 1 - Only the volatiles of the depleted mantle (DM, supposedly the most well-known) are considered; Case 2 - Volatiles of the bulk silicate mantle (BSM = DM+EM) are considered, as used recently by Sossi et al., (2020). The integration of multiple earlier MO stages, nebular capture processes, and impact degassing (Tucker and Mukhopadhaway, 2014) are not addressed here.

Case 1 implicitly considers that the deep enriched mantle was never involved in the last MO (Fig. 1). This assumption is consistent with the N, He and Ne isotopic signatures of plumes compared to MOR basalts (Tucker and Mukhopadhyay, 2014; Labidi et al., 2020). The mass of the DM is unspecified, but its CHNS concentrations as estimated in literature data (Table 1) are used here. The mass of the MO is set to that of the depleted mantle and is assumed to vary from 10^{27} to 3.10^{27}g (¼ to ¾ of the BSM) (Hofmann, 2003; Miller et al., 2019).

Case 2 relies on the fact that the bulk silicate Earth (BSE) was fully molten. The CHNS masses of the surface + bulk silicate mantle (BSM) were thus processed through the MO and its

atmosphere. In this context, the MO has the size and mass of the BSE. Sossi et al (2020) recently simulated a similar case at fO_2~IW+0.5. Because the amount of volatiles in the deep enriched mantle is much less well-known and debated, we considered both extreme options: a strongly (Marty, 2012) and a moderately enriched deep mantle (Hirschmann, 2018).

Table 1: the distribution of CHNS volatiles in the different Earth reservoirs and a summary of the run conditions used in our simulations.

Elements	Surficial reservoirs[1] (g)	Bulk Silicate Mantle BSM[2] (ppm)	Depleted Mantle DM[3] (ppm)
C after H 2018	1.06×10^{23}	110	37
after M 2020		211-646	
H after H 2018	1.7×10^{23}	33	15
after M 2012		100-300	
N	6.4×10^{21}	1.1	0.1-0.3
S	1.5×10^{22}	118-200	120-220

Runs with variable MO sizes

Cases	1. MO = DM + Surficial reservoirs[5]			2. MO = BSE + Surf. Res. [4]
MO size	¼ BSM	½ BSM	¾ BSM	BSM
C (ppm)	143	90	72	140-400
H (ppm)	191	102	73	79-333
N (ppm)	6.5	3.3	2.2	2.8
S (ppm)	126	123	120	119

Data after Hirschmann (2018) for the surficial reservoirs and the bulk silicate mantle (BSM). For C and H, the data of Marty al. (2020) have also been considered. Data after Marty et al. (2020) for N in the BSM and DM. The depleted mantle is after Saal et al. (2002) and Le Voyer et al (2017).
1: Mass of atmosphere + sediments + crust
2: Volatile contents in ppm-wt normalized to the bulk silicate Mantle (BSM = 4×10^{27} g)
3: Volatile contents in the depleted mantle
4: Here we considered that the entire CHNS content of Earth (surface + BSM) has been processed by an MO with the size of the bulk silicate Earth (BSM).
5: Here, we considered that the CHNS contents of the Earth's surface plus DM have been processed and the MO had the size of the DM.

3.

4. Mass balance and chemical equilibria calculations

The mass of the system (M^{tot}) is the sum of masses of both MO (M^{MO}) and its atmosphere (M^{MOATM}):

$$M^{tot} = M^{MO} + M^{MOATM} \quad (1)$$

The total mass fractions in C-H-N-S of the system were calculated as:

$$S_i^{tot} \times M^{tot} = S_i^M \times M^M + M_i^{ATM} = S_i^{MO} \times M^{MO} + S_i^{MOATM} \times M^{MOATM} \quad (2)$$

where i is the element, S_i^{tot} is the total mass fraction of the element i in the system, M^M represents the mass of the considered mantle (respectively BSM for case #2 and DM for case #1), S_i^M is the mass fraction of i in the considered mantle, and M_i^{ATM} the mass of element i in the present-day atmosphere+ocean+crust. S_i^{MO} and S_i^{MOATM} correspond to the mass fraction of the element i in the MO and its atmosphere, respectively.

In Case 1, we assumed $M^{MO} = M^{DM}$, implying that variable MO sizes change the total mass fractions of C-H-N-S of the system: the larger the DM (or MO) the larger the quantity of CHONS available to partition between the MO and its atmosphere (Table 1).

A gas-melt equilibrium is assumed to occur at the MO-atmosphere interface. This interface is characterized by a fixed temperature (1500°C, see figure S1 for a test on the effect of higher T), a varying oxygen fugacity (from IW-6 to IW+4) and a pressure (P^{MOATM}) given by:

$$P^{MOATM} = \frac{g \times m^{gas} \times M^{Mtot}}{4 \times \pi \times r^2} \quad (3)$$

Where *g* is the gravitational acceleration, 9.8 $m.s^{-2}$, m^{gas} is the mass fraction of gas in the system and r the radius of the planet. There is therefore no *a priori* assumption about the mass of the atmosphere formed, which is calculated from the abundances of volatile species in the system, the size of the planet and its MO, and g.

The relationship between the atmospheric pressure and the composition of the atmosphere is given as:

$$P^{atm} = \sum P_i = P_{CO2} + P_{CO} + P_{CH4} + P_{H2O} + P_{H2} + P_{N2} + P_{H2S} + P_{S2} + P_{SO2} \quad (4)$$

The relationship between gas partial pressure (P_i) and the content of dissolved species (S_i) in the melt is simplified to:

$$S_i = \sum a_i \times P_i^{b_i} \quad (5)$$

Where a and b are empirical constants specific to each species (see Supplementary methods). These constants were taken from Iacono-Marziano et al., (2012a) for H_2O-CO_2, Gaillard et al., (2003) and Hirschmann et al., (2012) for H_2, Armstrong et al., (2015) for CO, Bernadou et al., (2021) for N_2, and primarily O'Neill and Mavrogenes (2002) for sulfur (see Supplementary methods). Some approximation was necessary because none of these solubility laws were calibrated for the composition and high-T of the MO (see Supplementary methods).

Finally, these solubility laws are coupled to a gas speciation model that has been presented in previous work (see Iacono-Marziano et al., 2012b) and used to solve the equilibria involving the O_2 component and the following redox couples C/CO, CO/CO_2, H_2/H_2O, H_2S/SO_2, CH_4/CO (Holloway, 1987). The relationship between f_{O2} and Fe^{3+}/Fe^{2+} is taken from Kress and Carmichael (1991) in order to mass balance O between gas and melt.

The MO degassing code is available at http://calcul-isto.cnrs-orleans.fr/apps/planet/.

5. Results.

5.1. The speciation – f_{O2} relationships and its planetary significance

Here we provide a broad picture of the volatility and speciation of the C-O-H-N-S elements as a function of oxygen fugacity. Our results provide the gas species' partial pressures in the atmosphere (Fig. 3A), and the equilibrium speciation of the C-H-O-N-S dissolved in the MO (Fig. 3B) at the MO-atmosphere interface. The CHNS abundances and the MO mass considered correspond to case (1), MO= ½ BSM (Table 1). In the most reduced conditions, C (stable as graphite), N and S are not volatile and remain in the MO, while H is efficiently degassed (as H_2). In more detail, at fO_2 of about IW-6, the atmosphere is dominated by 40 bar H_2 with about 1 bar resulting from CH_4 outgassing (the CH_4 fraction should vary with C/H). In spite of the high H volatility, 100-200 ppm H_2O remains dissolved in the MO together with ~30 ppm H_2. This means that >50% of H remains dissolved in the MO even in the most reduced cases. As fO_2 becomes oxidizing, i.e. >IW, N_2, CO_2, H_2O and SO_2 become increasingly dominant in the system. In these conditions N_2 and CO_2 are highly volatile, while H_2O is still not due to its high solubility in silicate melts. Sulfur only becomes volatile at the uppermost f_{O2}, close to that of the present-day mantle. Moreover, with increasing fO_2, graphite and CH_4 are oxidized to CO, resulting in an increase in atmospheric pressure until graphite is exhausted. A pressure of ~80-90 bar is reached at fO_2 ~IW-3.5, when all graphite is oxidized (Fig.3). In a system containing more C, this threshold fO_2 is raised, as discussed in section 4.2. Consequently, reduced bodies, such as enstatite achondrite parent bodies or planet Mercury, must undergo surficial graphite

saturation as a rule. Given the low graphite density and the low C-solubility in silicate melts, this would explain the graphite-rich rocks observed by the Messenger mission to Mercury's surface (Charlier and Namur, 2019; Keppler and Gobalek, 2019). In contrast, under oxidizing MO conditions, i.e. > IW-2, all H remains dissolved as H_2O, while C is significantly outgassed. This has fundamental implications for the capacity of this MO to accrete under wet conditions: reduced, enstatite-like MO had ca. 30-40% of accreted H as H_2 in the vapour state, implying a greater exposure to H-loss to space (eg. Pahlevan et al., 2020; Katyal et al., 2020; H-escape or atmospheric blow), while more oxidized MOs were able to prevent their hydrogen inventory from escape, since >99% of their H was dissolved in the MO. In summary, a reduced MO can largely retain N, C, and S, as these elements are not efficiently degassed at low oxygen fugacity. An oxidized MO could evolve wet, while it must outgas most of its C and N. Sulfur outgassing is not expected unless under oxidized f_{O2} conditions similar to the present-day mantle.

5.2.Mass balancing the MO – Atmosphere CHONS distribution

On an element-by-element basis, we quantitatively discuss the MO - atmosphere mass transfers caused by the speciation relationships shown in figure 3. We first discuss Case 1 (MO = DM + atmosphere), and then Case 2 (MO = BSE).

Case 1: Melting the Depleted Mantle (Table 1)

Figure 4 illustrates Case 1, where the MO is the same size as the depleted mantle. In this figure, the masses of outgassed and preserved CHONS remaining dissolved in the MO are shown for variable f_{O2} conditions and variable MO sizes.

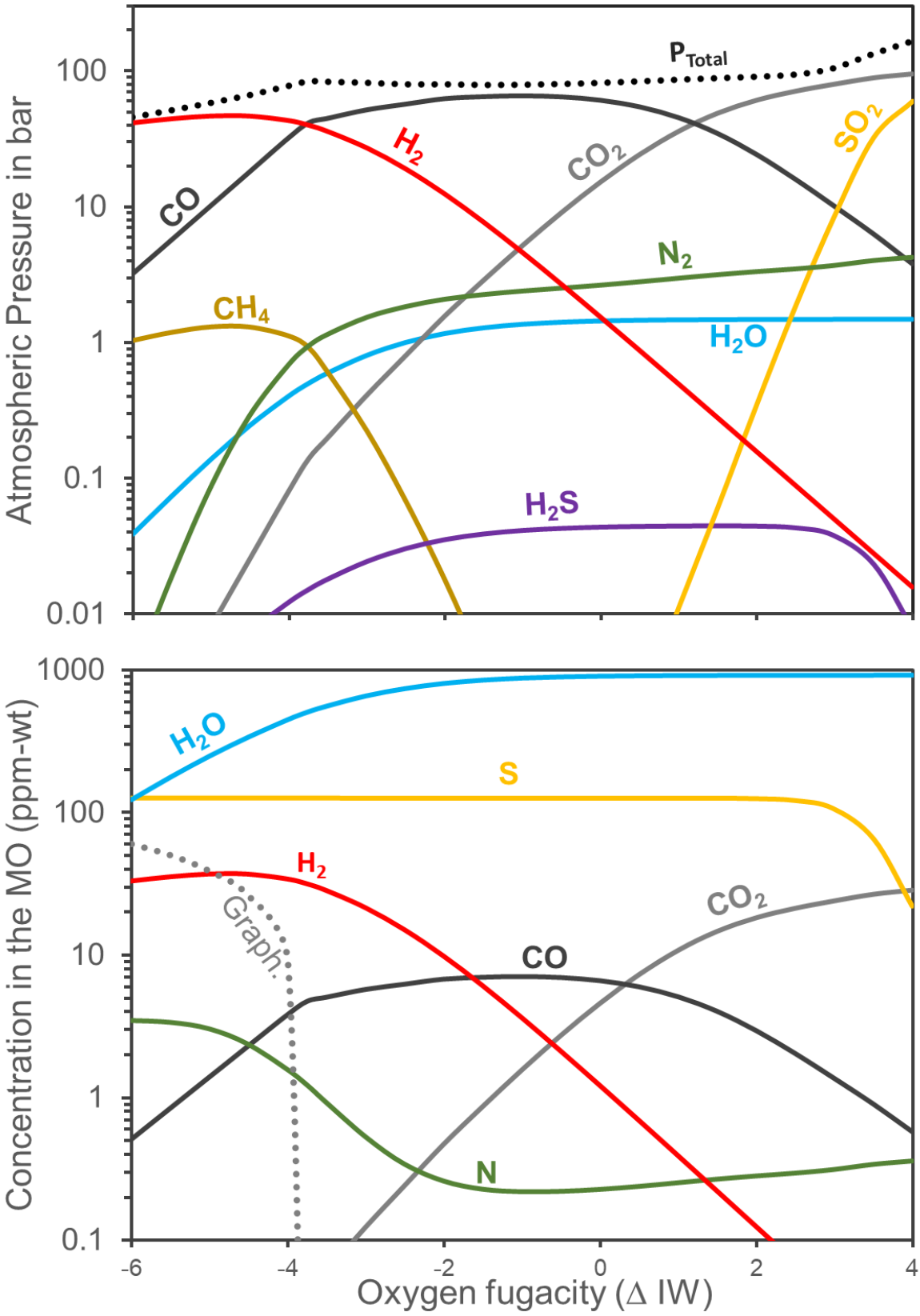

Figure 3. C-H-O-N-S speciation in the gas and the melt as a function of fO_2 during the MO – atmosphere equilibration (Case 1, ½ BSM in Table 1) at 1500°C. A: Partial atmospheric pressures and speciation of the C-H-O-N-S elements in the basal atmosphere. B: Concentration in ppm-wt of the C-H-O-N-S species dissolved in the shallow MO.

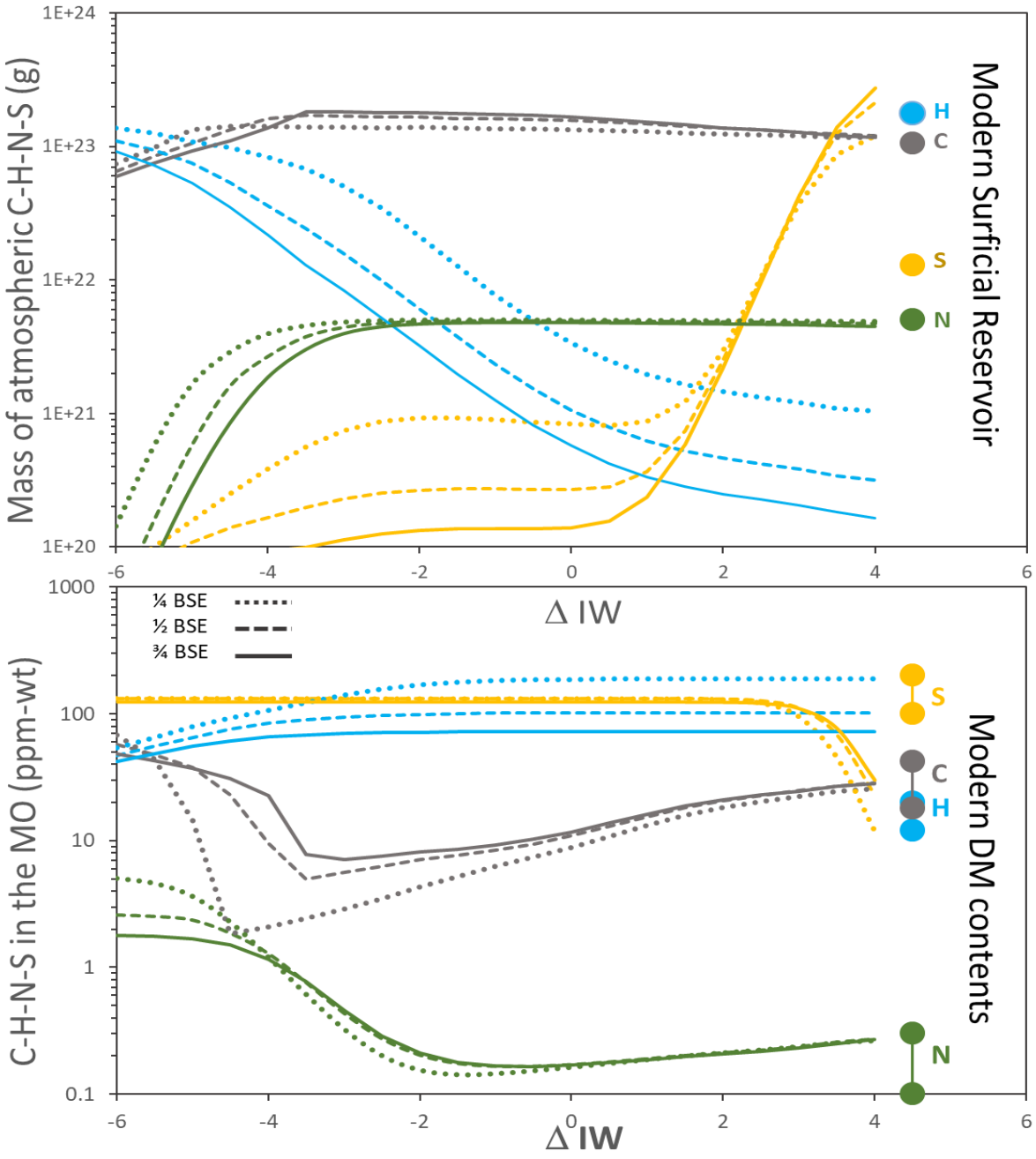

319

320 *Figure 4. Mass distribution of the C-H-O-N-S elements as a function of fO_2 during the MO –*
321 *atmosphere equilibration cases 1, DM = MO. Top: Calculated masses of C-H-O-N-S outgassed*
322 *in the MO atmosphere and comparison with the present-day surficial mass of C-H-N-S on*
323 *Earth. Bottom: Calculated concentrations of C-H-N-S (ppm-wt) in the shallow MO and*
324 *comparison with the present day CHNS content in the depleted mantle (DM).*

325 The present-day mass of carbon in the Earth's surficial reservoir is 1.06×10^{23} g (Hirschmann,
326 2018). Figure 4 indicates that the calculated mass of C outgassed from the MO varies slightly
327 with fO_2 but remains in the range 6.4×10^{22} – 1.7×10^{23} g. It should be noted that the outgassed
328 mass of C is insensitive to the mass of the MO. This calculated degassed C mass brackets,
329 within a 50% relative variation, the present-day mass of carbon in the Earth's surficial reservoir.

The carbon content in the depleted mantle is highly variable (19-1,200 ppm), but recent estimates give an average value of 37 ±12(1σ) ppm-wt (Le Voyer et al., 2017; Hirschmann, 2018). The calculated C content in the equilibrium MO varies from 2 to 70 ppm-wt depending on fO_2 and the size of the MO. At low fO_2 (<IW-3), graphite saturation implies that most C in the MO is present as graphite. At higher fO_2, C dissolves in the silicate melt as CO (fO_2<IW) and as CO_3^{2-} (at fO_2>IW+1) (see also Fig.3). The C-content of the MO perfectly matches the C content of the depleted mantle if degassing occurs at fO_2 >IW or at <IW-4. If degassing of the MO occurs at intermediate fO_2 (IW-4 / IW), the C-content of the MO is significantly lower (2-15 ppm C) than the average C-content of the depleted mantle (37±12 ppm C). When the large uncertainty in carbon content of the depleted mantle is propagated through the calculation, a moderate impact on the mass of outgassed C and on the C-content of the MO is observed (Fig. 5). Additional sensitivity tests are shown in Fig. 5A, using lower and higher bulk C contents (45-700 ppm C in the bulk system). All calculations converge at low fO_2, where graphite saturation occurs but the domain of graphite saturation changes with the bulk C content (the MO is systematically graphite-saturated in the C-rich case if fO_2<IW-1). In this C-rich system, the C-content of the MO can become as high as that of the enriched mantle (in both reduced and oxidized cases). The mass of outgassed C in such a case would be around 10^{25}g, (i.e. 10 times greater than the present-day surficial mass of C).

The present-day mass of nitrogen in the Earth's exosphere is 5×10^{21} g. The calculated mass of nitrogen outgassed by the MO is in the range of 6.3×10^{19} to 6.5×10^{21} g (for a total N mass of 7×10^{21} g for Case 1, ie. DM size= ½ BSM, Table 1). The lowest value was calculated for the lowermost fO_2 (Fig.4A). This indicates that MO outgassing at $fO_2 \geq$ IW-3 would yield an outgassed mass of N that matches the present-day Earth's surficial mass of N perfectly. The calculated N-content dissolved in the MO (Fig. 4B) varies with fO_2 from values greater than 1 ppm at <IW-4, to within the range 0.2-0.3 ppm N at fO_2>IW-2. The N content of the DM is currently estimated to lie within the range 0.1-0.3 ppm (Marty, 2020), which is similar to our prediction for the N-content in the MO at >IW-2. To summarise, we conclude that the present-day distribution of carbon and nitrogen between the Earth's surface and depleted mantle could have been attained by outgassing of the MO formed by the Moon-forming impact, if the fO_2 of the MO-atmosphere interface was ≥ IW-3. This could be coincidental, but the similarities are striking.

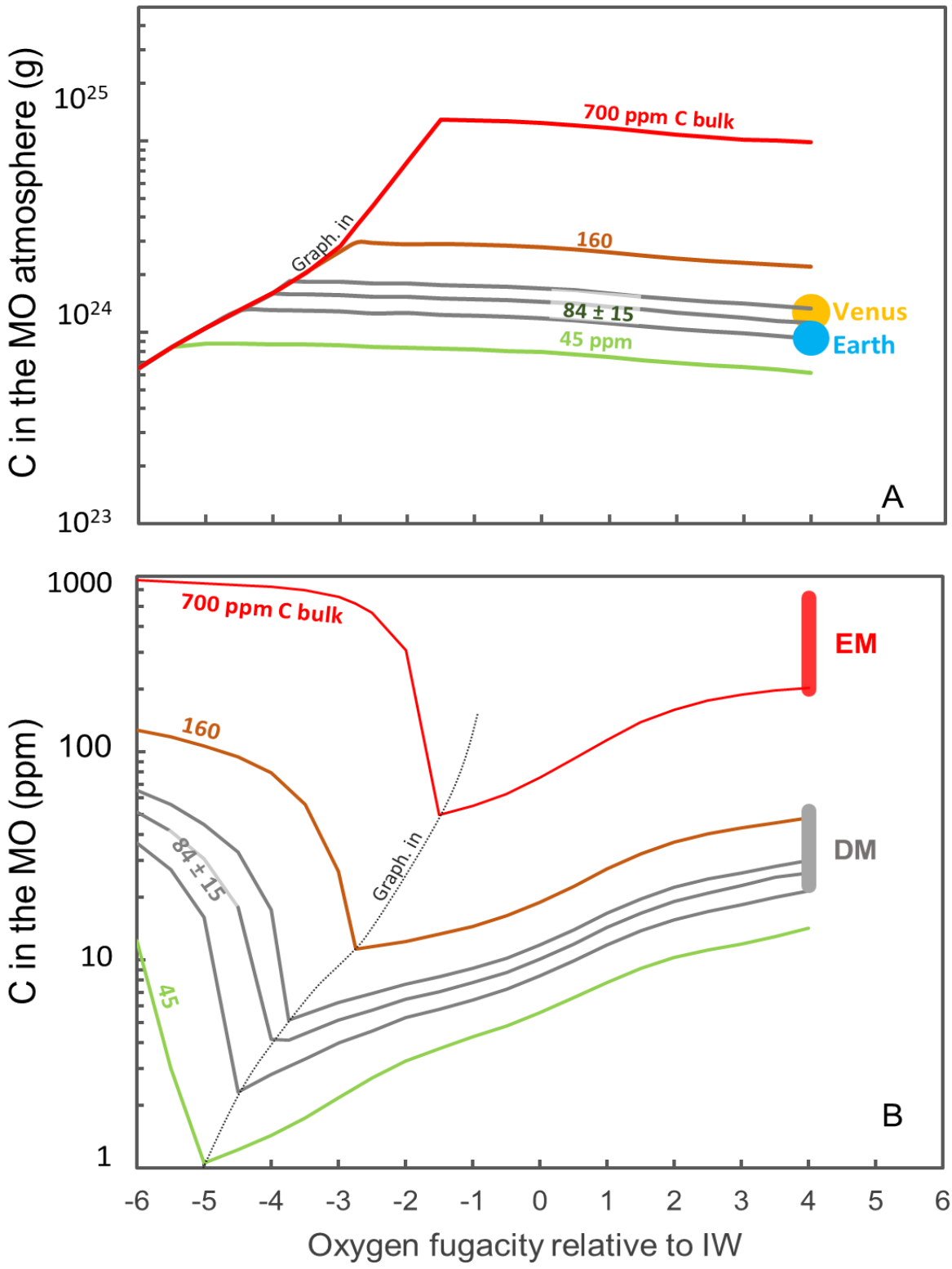

Figure 5. Sensitivity tests on the effect of bulk C-content on the partitioning of carbon between the MO and its atmosphere. The C-content of the depleted (DM) and the enriched mantle (EM) is shown for comparison in the bottom diagram while the C-mass of the Earth's and Venus's atmosphere are shown in the top diagram. The domain of graphite saturation is marked by the dashed line.

The present-day mass of hydrogen at the Earth's surface is 1.8×10^{23} g. At IW-6, the mass of outgassed H is $1.1\pm0.2\times10^{23}$ g, which makes up 60% of the present-day surficial mass of H (Fig. 4). Under such conditions, the H content of the MO is ca. 50 ppm (Fig. 3), which is equivalent to ~400 ppm H_2O. Massive degassing of hydrogen therefore requires strongly reducing conditions at the surface of the MO. In contrast, MO degassing at (even moderately) oxidizing conditions prevents the outgassing of hydrogen. Notably, degassing at the fO_2 of the present-day Earth's mantle would produce a dry atmosphere, containing 500 times less H than today. Interestingly, contrary to C and N, the H balance of outgassing/ingassing is affected by the size of the MO: smaller MOs tend to outgas more H (Fig. 4). This is because the atmospheric pressure is lower for small MOs. To summarize, apart from in strongly reduced conditions, hydrogen is hardly outgassed.

The present-day mass of sulfur at the Earth's surface is 1.2×10^{22} g (Canfield, 2004). The mass of outgassed S from the MO is strongly fO_2 dependant and remains well below 10^{22} g for fO_2 <IW+2, whereas at fO_2 of ca. IW+2.5, the amount of S outgassed by the MO would perfectly match the present-day surficial S budget (Fig.4). On the one hand, a negligible fraction of S is degassed if fO_2 <IW+2. On the other hand, at a surficial MO fO_2 similar to that of the present-day mantle (Armstrong et al., 2019), the outgassed mass of S would exceed the modern Earth's surficial sulfur content by an order of magnitude, leaving behind a sulfur-poor mantle.

Thus it can be seen that strongly atmophile elements such as C and N are unaffected by the size of the MO, whereas moderately atmophile elements, such as H and S, are more significantly affected. However, the most important parameter controlling CHNS outgassing remains the oxygen fugacity of the shallow magma ocean.

Case 2: Melting the Bulk Silicate Earth (Table 1)

Figure 6 illustrates calculated masses of outgassed CHONS for the case of a fully molten silicate Earth, together with the CHNS content of the MO in equilibrium with this atmosphere. For most fO_2 conditions, and for the two bulk C-contents considered (Hirschmann 2018 and Marty et al., 2020, respectively), the outgassed masses of C significantly exceed present-day Earth's surficial reservoir (by a factor of 5 to 10). The C-content in the MO lies within the range 20-300 ppm C, depending on the fO_2 and the bulk C-content. Such a concentration range is intermediate between the C-content of the depleted mantle and that of the deep enriched mantle. We therefore conclude here that a MO of the size of the BSE would produce an atmosphere and

a MO significantly exceeding the present-day C reservoirs of the Earth's surface and the depleted mantle.

The mass of outgassed hydrogen shows similar trends to Case 1, in that it decreases with increasing fO_2. Yet due to the much higher H content of the BSE compared to that of the DM (Hirschmann 2018 vs. Saal et al., 2003), we predict a much greater mass of outgassed H and a higher H content in the MO than for Case 1. The H content in the MO lies within the range of 50 to 330 ppm (ie. 450 – 3000 ppm H_2O), which largely exceeds the H content of the depleted mantle. The mass of outgassed H ranges from 7×10^{23} to 2×10^{20} g, which implies that a mass similar to the present-day Earth's surface (Mass H = 1.8×10^{23} g) may have been outgassed during the MO stage of Case 2.

The results for S and N are marginally different from those discussed in Case 1. It is of particular note, however, that the N contents in the MO always exceed the N content in the DM, whereas the mass of outgassed N approaches the present-day N surficial mass, though the agreement is not as striking as in Case 1.

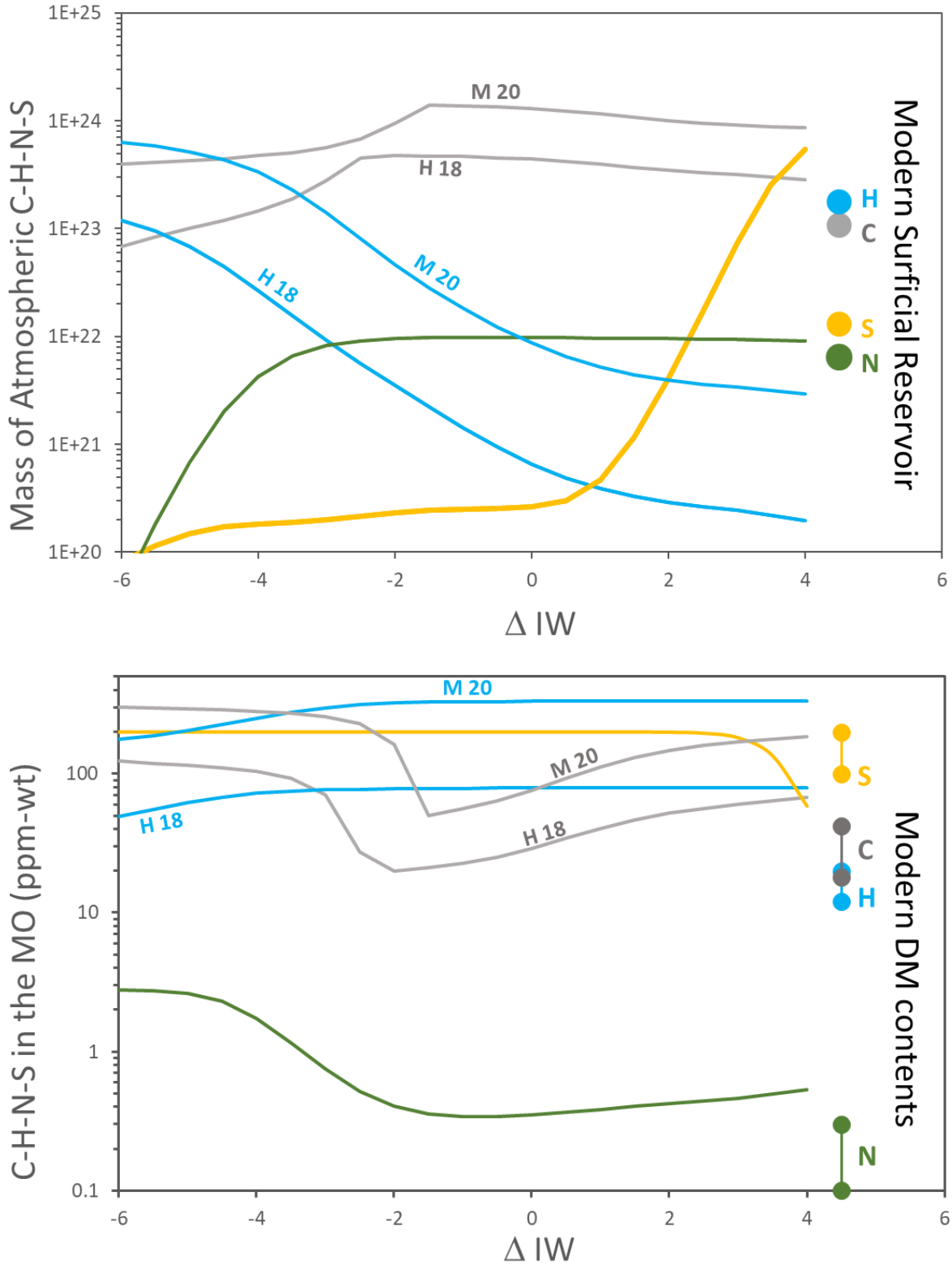

Figure 6. Mass distribution of the C-H-O-N-S elements as a function of fO_2 during the MO – atmosphere equilibration Case 2, BSE = MO. Top: Calculated masses of C-H-O-N-S outgassed into the MO atmosphere and comparison with the present-day surficial mass of C-H-N-S on Earth. Bottom: Calculated concentration in C-H-N-S (ppm-wt) in the shallow MO and comparison with the present day CHNS content in the depleted mantle (DM). H 18 refers to Hirschmann (2018) and M 20 refers to Marty et al (2020).

6. Discussion.

6.1. Melting the BSE.

Case 2 involves the partitioning of COHNS elements between the MO and its atmosphere, and assumes that the BSE was once fully molten. We found the abundance of all elements, in both the atmosphere and MO, exceeded that of the present-day surficial and DM reservoirs. Though this might be interpreted as a circular reasoning (because the way the BSE C-H-N-content has been estimated implies the existence of deep reservoirs, see Hirschmann, 2018 and Marty et al., 2020), this experimental scenario suggests that a hidden (deep) sink must have formed either during the solidification of the MO or during the subsequent 4.5 Gyrs of mass transfer governed by mantle geodynamics (eg. Ballmer et al., 2017). This deep reservoir is also required by independent CHNS-noble gas isotopic constraints (eg. Tucker and Mukhopdhay, 2014; Labidi et al., 2020). Given that our model does not address mass transfer processes conducive to deep CHNS reservoirs, there is no purpose in looking at Case 2 in more detail. We simply state that our calculations define the starting distribution of CHONS elements prior to MO solidification (Fig.6). These starting conditions could then be used in geodynamical models addressing volatile mass transfer during MO solidification and subsequent geodynamic processes.

Recently, Sossi et al. (2020) conducted similar calculations, and estimated the atmospheric pressure resulting from vaporisation of the BSE volatiles at fO_2 close to IW. Case 2, using the BSE values of Hirschmann (2018), at fO_2 of IW, is similar to the case studied by Sossi et al. (2020). Accordingly, the estimations of atmospheric pressure only slightly differ between the two studies (P^{atm} = 220 bar in the present study compared to 190 bar in Sossi et al., 2020). The small difference might be related to the use of different solubility laws for N_2 and CO_2 and/or that H_2 and CO solubility laws are neglected in Sossi et al. (2020).

6.2. Does the depleted mantle delineate the MO?

The atmosphere / MO distributions of carbon and nitrogen perfectly match the present-day surficial / DM ones if fO_2>IW-2. This may be purely coincidental, yet the fingerprint of the MO outgassing stage for the most volatile elements is striking. If true, the C-N mantle and surficial reservoirs created following MO degassing seem to have been only marginally affected by 4.5 Gyrs of mantle geodynamics. The present-day outgassing rates for nitrogen are very low and would require longer than the Earth's lifetime to build the surficial N reservoir (Hirschmann, 2018). This corroborates our finding that the N surficial budget was set by the primordial N outgassing. Present-day outgassing rates for carbon, on the other hand, are much

greater, enabling the surficial reservoir to be refilled within the time-scale of the Earth's lifetime (Hirschmann, 2018). We propose that a steady state balance between ingassing and outgassing may have operated over geological eons. The C content of the DM mantle would then be directly inherited from the C content of the degassed MO as defined in Figure 4, which has been (and continues to be) progressively enriched by subducted C-rich lithospheric slabs. The C content of the DM must therefore have increased over time. In this context, MORB samples these heterogeneities but remains broadly dominated by strongly C-depleted lithology (Le Voyer et al., 2017).

6.3. Earth—Venus MO atmospheres

As also noted by Sossi et al. (2020), our results indicate that atmospheres calculated under moderately reducing conditions (i.e. IW-2< fO_2 < IW+2) broadly share many features with the modern atmosphere of Venus (though the bulk volatile budget is based on the Earth's reservoir). Calculated atmospheres are dry, with CO or CO_2 pressure of about 80-220 bar, N_2 pressure of about 2-4 bar, and only small amounts of sulfur (Fig. 3). In particular, degassing of Earth's MO in Case 1 (melting of the DM) produces an atmosphere that perfectly matches the Venusian one (see Table 1 and Fig. 3), which differs from the conclusions of Sossi et al. (2020) in which melting of the BSE is used. We recall here the striking Earth-Venus similarities in terms of surficial reservoirs. The mass of carbon in Venus's atmosphere is 1.25×10^{23} g and the Earth's surface contains 1.03×10^{23} g C. The mass of nitrogen in Venus's atmosphere is 4.8×10^{21} g and Earth's surficial mass of nitrogen is estimated to be 5×10^{21} g. This corroborates the multiple similarities already noted elsewhere (Kasting et al., 1988; Lecuyer et al., 2000; Wordsworth 2016; Gilman et al. 2020; Sossi et al., 2020) between planet Earth and Venus. It may also indicate that, for both planets, the carbon and nitrogen surficial inventories were likely formed during the MO stage. However, the present-day forms of surficial C and N differ on the two planets. This is because a range of biotic and abiotic mechanisms have fixed C and N in the Earth's soil, sediments and crust, but since these mechanisms did not operate on Venus (Worsdworth, 2016) these elements remained in Venus's atmosphere. This is likely related to the presence of liquid water on the Earth's surface and its absence on Venus.

The divergence in composition of the atmospheres of Venus and Earth has long been discussed in terms of distance to the Sun, which has major effects on atmospheric temperatures and hydrogen escape processes (Kasting, 1988; Hamano et al., 2013; Gillmann et al., 2020). Here, our redox analysis shows that degassing under oxidized conditions (ie. fO_2> IW-2) prevents H

emission into the atmosphere. The atmosphere is therefore dominated by C and N species with total atmospheric pressures of ca. 80-200 bar (according to the MO sizes and the volatile contents investigated in this study). This may define a Venusian scenario, in which the atmosphere was dry from the beginning (ie. it contains ca. 1% H_2O, Figure 2, see also Sossi et al., 2020). Conversely, degassing under reduced conditions produces an atmosphere that is significantly enriched in hydrogen. Such reduced degassing conditions are possible if the surface of the MO is graphite-saturated because of floatation processes (ie. Keppler and Gobalek, 2019). However, this does not mean that the whole MO is subject to graphite-saturation or the same degree of reducing conditions. For example, one may consider a MO that is overall at IW (eg. Sossi et al., 2020) that is C-saturated at the surface because of graphite floatation (Keppler and Gobalek, 2019). As pressure decreases, graphite-gas equilibria can buffer fO_2 as low as IW-5 at P<10 bar, whereas the same system at P> 1000 bar would buffer fO_2 ~ IW-2 (Fig. 2, see Iacono-Marziano et al., 2012). This graphite-saturated case may define a terrestrial scenario, in which the atmosphere was H-rich from the beginning, ie. containing half to $1/10^{th}$ of the present-day amount of the Earth's surficial water (Fig. 4), which in turn implies that a significant amount of H remains in the MO. The transition from a strongly reducing to a moderately oxidizing situation may be viewed in the framework of hydrogen escape processes (Kasting, 1988; Hamano et al., 2013; Gillmann et al., 2020). In this context, a more efficient H-loss on Venus as compared to Earth must have caused a shift toward more oxidizing conditions (ie. H_2-loss). Such loss must also consider that a large fraction of the H remains dissolved in the MO, which is not taken into account in such models (eg. Katyal et al., 2020). In a scenario where Earth and Venus have received similar quantities of CHONS during accretion (eg. Gillman et al., 2020 and ref. therein), an atmospheric divergence during the MO stage is possible. This would be due to enhanced H-loss on Venus, which increased fO_2 and H solubility in the MO. In other words, both H-loss and H-incorporation in the MO may have contributed to the drying of the Venusian atmosphere. It seems unlikely that post-MO-stage degassing would alter this conclusion, as detailed in section 5.5.

6.4. Cooling, solidification and degassing of the MO

In the absence of experimental data, the effect of temperature remains difficult to define on the solubility of volatiles at T>1300°C. In figure S1, we illustrate a moderate effect calculated over the T range 1500-2000°C. Graphite saturation is, however, significantly enhanced as T

decreases. This implies high atmospheric pressures at high T, even for very low fO_2 conditions, in contrast to the data shown in Figure 4. Maintaining high atmospheric pressure makes hydrogen less volatile. However, we must keep in mind that there is no constraint on the effect of T on H_2 and H_2O solubility in mafic compositions.

The question of the extent of CHONS outgassing or ingassing during solidification of the MO is beyond the scope of this study. Nevertheless, some aspects must be discussed here because the incompatible nature of hydrogen might have enhanced its degassing during MO crystallization. Figure S2 shows the calculation of an upper bound assuming perfect crystal settling and incompatible behaviour for C-H-N during the solidification of the MO. Following 90% crystallisation in an extreme configuration such as this, the H-content in the residual melt can reach 0.5-0.7wt%, but H outgassing would remain moderate. Furthermore, Hier-Majumder and Hirschmann (2017) calculated that the entrapment of water-rich interstitial melt at the MO crystallization front could limit the extent of H-enrichment in the residual liquid of a solidifying MO. It therefore appears that the process of MO solidification itself would not necessarily enhance hydrogen outgassing. Significant hydrogen degassing at the MO stage seemingly requires strongly reduced conditions and the entrapment of a major part of the primordial water in the deep mantle is very likely. This implies that early hydrated komatiites (3.3 Ga, Sobolev et al., 2019) may not require early subduction processes.

6.5. Post-MO outgassing

Once the MO solidified, mantle convection and associated volcanism may have contributed to the degassing of the planetary interior. Gaillard and Scaillet (2014) have shown that the degassing of magmatic water is limited by a dense atmosphere such as that formed by the MO. If water remained trapped in the mantle after the magma ocean stage, the basalt produced by melting of post-magma-ocean mantle containing 300-600 ppm (Table 1), could emit a gas phase containing ca. 10% H_2O at ca. 100 bar. In contrast, in a 1-bar atmosphere, the gas phase would be dominated by H_2O. Carbonate precipitation may reduce the amount of atmospheric CO_2 and decrease the atmospheric pressure, but this would require the presence of oceans (Sleep, 2011) and therefore the outgassing of H at an earlier stage. This should be addressed by specific studies in the future, but it appears that if hydrogen was not degassed from the MO, the atmosphere would have likely remained dry.

549 Finally, in most cases discussed here, sulfur is not degassed from the MO. Only an unexpectedly
550 highly oxidizing MO could significantly outgas sulfur. Here again, MO solidification would
551 not significantly increase the mass of degassed sulfur because sulfur is strongly compatible in
552 sulfides and the high density of molten sulfides would cause deep S sequestration. Sulfur
553 outgassing associated to post-MO volcanism (Gaillard et al., 2011) must thus be considered,
554 although a quantitative assessment of the amount of sulfur outgassed during the Archaean is
555 beyond the scope of this paper.

556 ## 7. Conclusions

557 The influence of oxygen fugacity on the degassing of the MO is quantified in this study.
558 Varying the fO_2, MO size and volatile content results in a great diversity of primary atmosphere
559 composition. Two end-member cases can be distinguished: oxidizing and reduced. In the
560 oxidizing case, C-N-S are outgassed from the MO, leaving an S-poor mantle, whereas H is not
561 volatile and is likely efficiently entrapped in the mantle during MO solidification. In the reduced
562 case, C-H±N are outgassed from the MO. We suggest that the deep enriched mantle (with
563 primordial He and Ne) was probably not involved in the last MO stage and represents a
564 fossilized pre-moon forming impact (Fig. 1). The last MO degassing most likely defined the C-
565 N distributions between the Earth's surface and the depleted mantle. Moderate post MO
566 recycling of surficial C via subduction of oceanic lithosphere may explain the heterogeneities
567 in C contents (and other trace and isotope elements) of the depleted mantle.

568 The surficial masses of C and N are identical on Venus and Earth and were most likely formed
569 during the MO degassing. The Earth-Venus divergence, with Venus's surface evolving to be
570 dry, may be linked to H-loss during the MO stage, which counterintuitively implies that the
571 interior of Venus could be wetter than its counterpart, the Earth. Finally, the geological
572 processes that are taken to define a habitable world must include the MO's central role in
573 generating the initial range of planetary environments.

8. References.

Armstrong, K., et al. Deep MO formation set the oxidation state of Earth's mantle. Science 365, 903-906 (2019) DOI: 10.1126/science.aax8376

Armstrong, L.S., et al., The speciation of carbon, nitrogen, and water in magma oceans and its effect on volatile partitioning between major reservoirs of the Solar System rocky bodies. Geochimica et Cosmochimica Acta 171, 283-302 (2015)

Ballmer, M. D., Houser, C., Hernlund, J. W., Wentzcovitch, R. M. & Hirose, K. Nat. Geosci. 10, 236–240 (2017).

Bernadou F, Gaillard F, Füri E, Marrocchi Y, Slodczyk A., Nitrogen solubility in basaltic silicate melt-Implications for degassing processes. Chemical Geology, 573, 120192 (2021)

Canfield, D.E. The evolution of the Earth surface sulfur reservoir. AJS Online 304, no. 10, 839-861 (2004) doi: 10.2475/ajs.304.10.839

Catling, D.C., Zahnle, K.J. The Archean atmosphere. Science Advances 6, no. 9, eaax1420, DOI: 10.1126/sciadv.aax1420 (2020)

Charlier, B., Namur, O. The Origin and Differentiation of Planet Mercury. Elements 15, 9-14 (2019)

Donnelly, K. et al., Origin of enriched ocean ridge basalts and implications for mantle dynamics. Earth and Planetary Science Letters 226, 347-366. DOI: 10.1016/j.epsl.2004.07.019 (2004)

Elkins-Tanton, L.T. Magma Ocean in the inner solar system. Annu. Rev. Earth Planet. Sci. 40, 113–39 (2012) doi: 10.1146/annurev-earth-042711-105503

Gaillard, F., Scaillet, B., and Arndt, N.T. Atmospheric oxygenation caused by a change in volcanic degassing pressure, Nature, 478, 229-232 (2011)

Gaillard, F., Scaillet, B. A theoretical framework for volcanic degassing chemistry in a comparative planetology perspective and implications for planetary atmospheres. Earth and Planetary Science Letters 403, 307–316 (2014).

Gaillard, F., Schmidt, B.C, MacCammon, C., Mackwell, S.J. Rate of hydrogen-iron redox exchange in silicate melts and glasses. Geochim. Cosmochim. Acta 67, 2427-2441 (2003).

Gaillard F., Bouhifd M.A., Füri E., Malavergne V., Marrocchi Y., Noack L. The Diverse Planetary Ingassing/Outgassing Paths Produced over Billions of Years of Magmatic Activity. Space Science Reviews 217 (1), 1-54 (2021).

Gillman, C., et al. Dry late accretion inferred from Venus's coupled atmosphere and internal evolution. Nature Geoscience 13, 265–269 (2020)

607 Greenwood, R.C., Barrat J-A, Miller M.F., et al. Oxygen isotopic evidence for accretion of
608 Earth's water before a high-energy Moon-forming giant impact. Science Advances, 2018; 4
609 (3): eaao5928 DOI: 10.1126/sciadv.aao5928
610 Grewal, D.S., Dasgupta, R., Farnell, A. The speciation of carbon, nitrogen, and water
611 in magma oceans and its effect on volatile partitioning between major reservoirs of the Solar
612 System rocky bodies. Geochimica et Cosmochimica Acta (2020), doi:
613 https://doi.org/10.1016/j.gca.2020.04.023
614 Hamano, K., Abe, Y., Genda, H. Emergence of two types of terrestrial planet on solidification
615 of magma ocean. Nature 497, 607-610 (2013) DOI :10.1038/nature12163.
616 Hier-Majumder, S., Hirschmann, M.M. The origin of volatiles in the Earth's mantle.
617 Geochemistry, Geophysics, Geosystems 18, 3078–3092 (2017)
618 Hirschmann, M.M., Dasgupta, R. The H/C ratios of Earth's near-surface and deep reservoirs,
619 and consequences for deep Earth volatile cycles. Chem. Geol. 262, 4-16 (2009)
620 Hirschmann, M.M., et al. Solubility of molecular hydrogen in silicate melts and consequences
621 for volatile evolution of terrestrial planets. Earth and Planetary Science Letters 345-348 38–
622 48 (2012)
623 Hirschmann, M.M., Comparative deep Earth volatile cycles: The case for C recycling from
624 exosphere/mantle fractionation of major (H_2O, C, N) volatiles and from H_2O/Ce, CO_2/Ba, and
625 CO_2/Nb exosphere ratios. Earth Planet. Sci. Lett. 502, 262–273 (2018)
626 Hofmann, A.W. Sampling Mantle Heterogeneity through Oceanic Basalts: Isotopes and Trace
627 Elements (2003) 10.1016/B0-08-043751-6/02123-X
628 Holloway, J. R., 1987. Igneous fluids. Rev. Mineral. Geochem. 17: 211–233
629 Iacono-Marziano G., Morizet Y., Le-Trong E., Gaillard, F. New experimental data and semi-
630 empirical parameterization of H_2O-CO_2 solubility in mafic melts. Geochim. Cosmochim. Acta
631 97, 1-23 (2012a) doi: 10.1016/j.gca.2012.08.035.
632 Iacono-Marziano, G., et al. Extremely reducing conditions reached during basaltic intrusion in
633 organic matter-bearing sediments. Earth and Planetary Science Letters 357, 319-326 (2012b).
634 Kasting, J.F. Runaway and moist greenhouse atmospheres and the evolution of Earth and
635 Venus. Icarus 74, 472-494 (1988).
636 Katyal, N., et al., Effect of mantle oxidation state and escape upon the evolution of Earth's MO
637 atmosphere. Astronomy & Astrophysics. (2020) DOI: 10.1051/0004-6361/202038779
638 Kelemen, P.B., Manning, C.E. Reevaluating carbon fluxes in subduction zones, what goes
639 down, mostly comes up. PNAS, (2015) doi/10.1073/pnas.1507889112

Keppler, H., Golabek, G. Graphite floatation on a magma ocean and the fate of carbon during core formation. Geochem. Persp. Let. 11, 12-17 (2019) doi: 10.7185/geochemlet.1918.

Kress V. C., Carmichael, I. S. E. (1991) The compressibility of silicate liquids containing Fe_2O_3 and the effect of composition, temperature, oxygen fugacity and pressure on their redox states. Contrib. Mineral. Petrol. 108, 82–92.

Labidi, J., et al. Hydrothermal $^{15}N^{15}N$ abundances constrain the origins of mantle nitrogen. Nature 580, 367–371 (2020). https://doi.org/10.1038/s41586-020-2173-4.

Le Voyer, C., et al., Heterogeneity in mantle carbon content from CO_2-undersaturated basalts. Nature Communications 8, 14062 (2017)

Lebrun, T., et al. Thermal evolution of an early magma ocean in interaction with the atmosphere. J Geophys Res (Planets) 118, 1155-1176 (2013)

Lécuyer, C., Simon, L., Guyot, F. Comparison of carbon, nitrogen and water budgets on Venus and the Earth. Earth and Planetary Science Letters 181. 33-40 (2000) DOI: 10.1016/S0012-821X(00)00195-3.

Marty, B., Alexander CMOD, Raymond SN, Primordial origins of Earth's carbon. Reviews in Mineralogy and Geochemistry, 75, 149-181 (2013)

Marty B., Almayrac M., Barry P., Bekaert D., Broadley M., et al. An evaluation of the C/N ratio of the mantle from natural CO_2-rich gas analysis: Geochemical and cosmochemical implications. Earth and Planetary Science Letters, 551, pp.116574. (2020) DOI: ff10.1016/j.epsl.2020.116574ff.

Marty, B., et al. Origins of volatile elements (H, C, N, noble gases) on Earth and Mars in light of recent results from the ROSETTA cometary mission. Earth and Planetary Science Letters 441, 91-102 (2016)

Miller, W.G.R., et al. Estimating the carbon content of the deep mantle with Icelandic melt inclusions. Earth and Planetary Science Letters 523, 115699 (2019) doi.org/10.1016/j.epsl.2019.07.002

O'Neill, H. St., Mavrogenes, J.A. The sulfide capacity and the sulfur content at sulfide saturation of silicate melts at 1400 C and 1 bar. J. Petrol. 43, 1049–1087 (2002).

Pahlevan, Kaveh & Schaefer, Laura & Hirschmann, Marc. (2019). Hydrogen isotopic evidence for early oxidation of silicate Earth. 10.31219/osf.io/2wc98.

Piani L., Marrocchi Y., Rigaudier T., Vacher L.G., Thomassin D., Marty B. Earth's water may have been inherited from material similar to enstatite chondrite meteorites. Science, Vol. 369, Issue 6507, pp. 1110-1113 (2020)

673 Rubie, D.C., et al. Accretion and differentiation of the terrestrial planets with implications for
674 the compositions of early-formed Solar System bodies and accretion of water. Icarus 248, 89–
675 108 (2015)
676 Saal, A.E., Hauri, E.H., Langmuir, C.H., Perfit, M.R.. Vapour undersaturation in
677 primitive mid-ocean-ridge basalt and the volatile content of Earth's upper mantle.
678 Nature 419, 451-455 (2002).
679 Sarafian, A.R., Nielsen, S.G., Marschall, H.R. et al. Early accretion of water in the inner solar
680 system from a carbonaceous chondrite–like source. Science 346, 623–626 (2014).
681 Sleep, N.H. The Hadean-Archaean environment. Cold Spring Harb Perspect Biol. 2(6):a002527
682 (2011) doi:10.1101/cshperspect.a002527
683 Sobolev, A.V., Asafov, E.V., Gurenko, A.A. *et al.* Deep hydrous mantle reservoir provides
684 evidence for crustal recycling before 3.3 billion years ago. *Nature* **571,** 555–559 (2019).
685 https://doi.org/10.1038/s41586-019-1399-5
686 Sossi, P.A., et al. Redox state of Earth's MO and its Venus-like early atmosphere. (2020) DOI:
687 10.1126/sciadv.abd1387.
688 Tucker, J.M., Mukhopadhyay, S. Evidence for multiple magma ocean outgassing and
689 atmospheric loss episodes from mantle noble gases. Earth and Planetary Science Letters 393,
690 254-265 (2014).
691 Wade, J, Wood, B.J. Core formation and the oxidation state of the Earth. Earth and Planetary
692 Science Letters 236 78-95 (2005)
693 Wordsworth, R. D. Atmospheric nitrogen evolution on Earth and Venus. Earth and Planetary
694 Science Letters 447,103–111 (2016).
695
696 **Acknowledgements**. This research is supported by the GASTON project (ANR-18-CE31-
697 0021). G.R. is supported by the VOLTAIRE project (ANR-10-LABX-100-01).
698 Correspondence and material requests should be addressed to F.G.: fabrice.gaillard@cnrs-
699 orleans.fr.
700

Supplementary Methods.

The relationship between gas partial pressure (P_i) and the content of the gas (S_i) in the melt is simplified as:

$$S_i = \sum a_i \times P_i^{b_i} \quad (6)$$

Where a and b are empirical constants specific to each species that the I component could form in the silicate. H_2O solubility is independent of the melt composition, while CO_2 solubility depends merely on the degree of polymerisation of the melt (Iacono-Marziano et al., 2012a). Since no experimental data defines the CO_2 solubility in molten peridotite, we used the estimation for komatiites of Iacono-Marziano et al. (2012a):

$$S_{CO2} = 1.1 \pm 0.15 \times P_{CO2} \quad (7)$$

For H_2 solubility, we used a combination of low pressure (Gaillard et al., 2003) and high pressure (Hirschmann et al., 2012) data. This yielded the following relationships with a 20% accuracy on the calculated S_{H2}:

$$S_{H2} = \exp(-(1.51 + P_{tot} \times \frac{9.43}{RT})) \times P_{H2} \quad (8)$$

The CO solubility law was taken from Armstrong et al. (2015) that we verified to be consistent with recent data (Yoshioka et al. 2019). The solubility law of Bernadou et al. (2020) was used for nitrogen.

$$[S_N] = K_1 \times P_{N2} + {fO_2}^{-3/4} \times K_2 \times {P_{N2}}^{1/2} \quad (9)$$

Where K_1 and K_2 are two thermodynamic constants fitted to account for the P and T dependences of N solubility. These constants have long been established (Libourel et al., 2004) at 1400°C, 1 bar in the C-O-N system, and Bernadou et al. have shown that eq. (8) remains almost unchanged from 1 atm to 3000 bar in the C-H-O-N system.

For sulfur, we used the following relationship:

$$Ln\,(S_S) = 13.8426 - \frac{26.476 \times 1000}{T_k} + 0.124 \times S_{FeO} + 0.5 \times Ln\,(\frac{f_{S2}}{f_{O2}}) \quad (10)$$

S_{FeO} stands for the concentration of iron (as FeO wt%) in the silicate melt. This equation is a rearrangement of the model used in O'Neill and Mavrogenes (2002) that has been refitted for the FeO content in the melt in wt% and the temperature in K. To calibrate equation (10), we used 369 experimental data from 9 papers (Haughton et al., 1974; Buchanan and Nolan, 1979;

729 Danckwerth et al., 1979; Gaetani and Grove, 1997; O'Neill and Mavrogenes, 2002; Ripley et
730 al., 2002; Bockrath et al., 2004; Zajacz et al., 2013; Mungall and Brenan, 2014; Nash et al.,
731 2019), linking sulfur content in silicate melts equilibrated with gas at 1 atm having known
732 values of fO_2 and fS_2, in the fO_2 range IW-1 to FMQ+0.1.

733 It must be clarified that none of these solubility laws has been directly calibrated for a peridotite
734 melt composition and at MO temperatures because of technical challenges for quenching such
735 compositions. This gives room for future improvement of the model and also introduces some
736 unknowns. We consider that the solubility laws for each species (eq. 5, 7-9) may be affected by
737 50% uncertainties due to this bias. This directly translates into 10-50% uncertainties in the
738 calculated concentrations of species in the melt and gas depending on the species considered,
739 which does not affect our conclusion given that solubility laws differ by orders of magnitude.

740 We only considered the stable species at the pressure and temperature prevailing at the MO-
741 atmosphere interface. In the MO atmosphere, however, one expects a thermal gradient from the
742 hot base to the cold upper regions. This must cause a change in the gas speciation with CH_4 and
743 H_2O dominating in the upper (colder) atmosphere while H_2-CO are stable at the (hot) base;
744 similarly, NH_3, which is negligible (<0.1% of total N) at high temperature, would be stabilized
745 in the upper (cold) atmosphere. Finally, a variety of CHONS speciations are expected in the
746 melt subject to high pressure in the deep MO (Armstrong et al., 2015; Grewal et al., 2020), but
747 the gas-melt equilibria that interests us occurs at low pressure (eg. tens to hundreds bar) and no
748 speciation data contradicts our assumptions at such conditions.

749

750

751

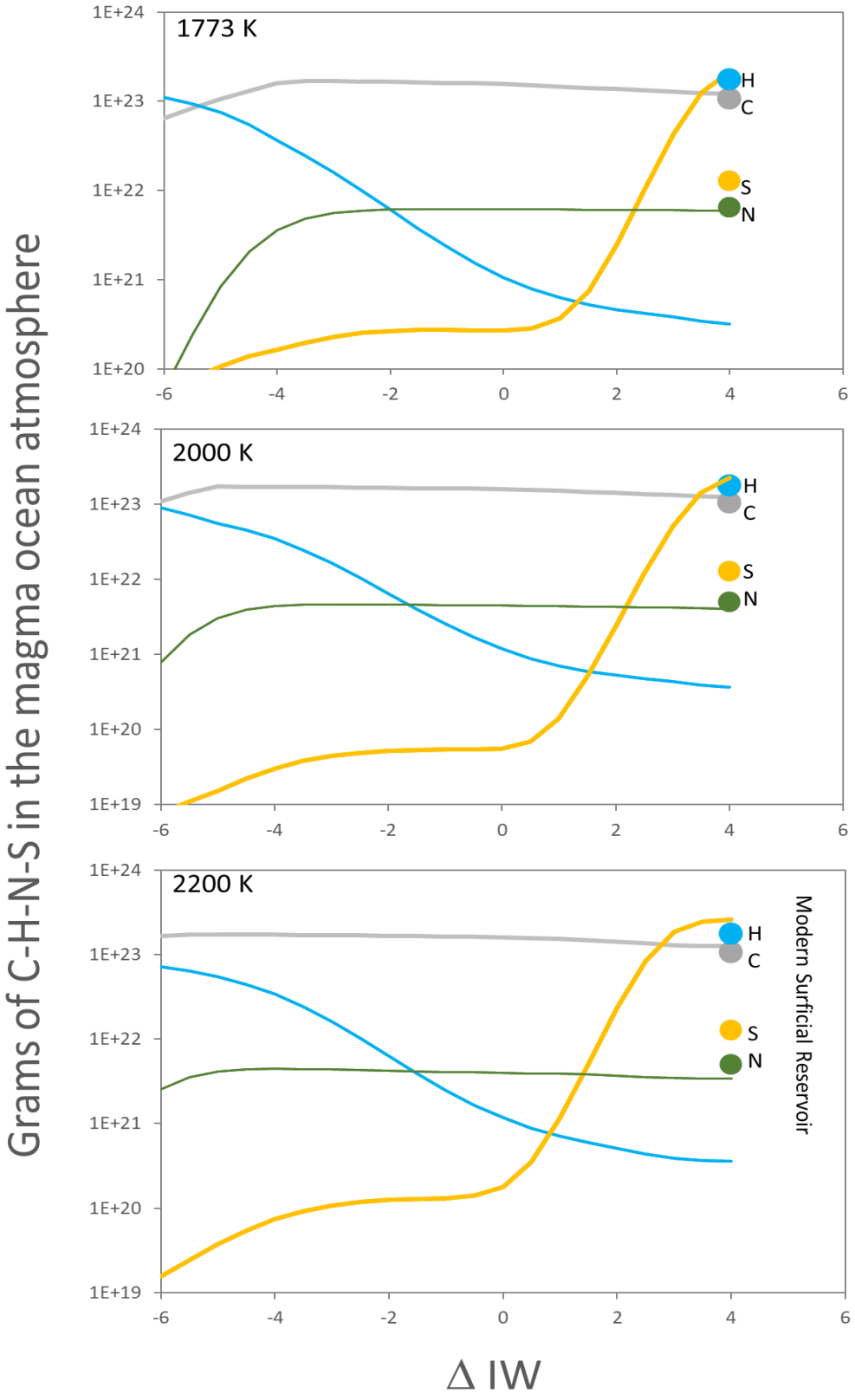

Figure S1. *The effect of temperature on the mass of outgassed CHNS from the MO. We illustrate here Case 1 with ½ BSM, (see table 1) at 1500°C - 1927 °C. We see that the calculated effect of T is moderate, which we must essentially attribute to our poor knowledge of the T-dependence of volatile solubility in basalts. In detail, we see that the low fO_2 domain of graphite saturation tends to disappear as T increases. This is because C dissolves more in both gas and silicate melt with increasing T.*

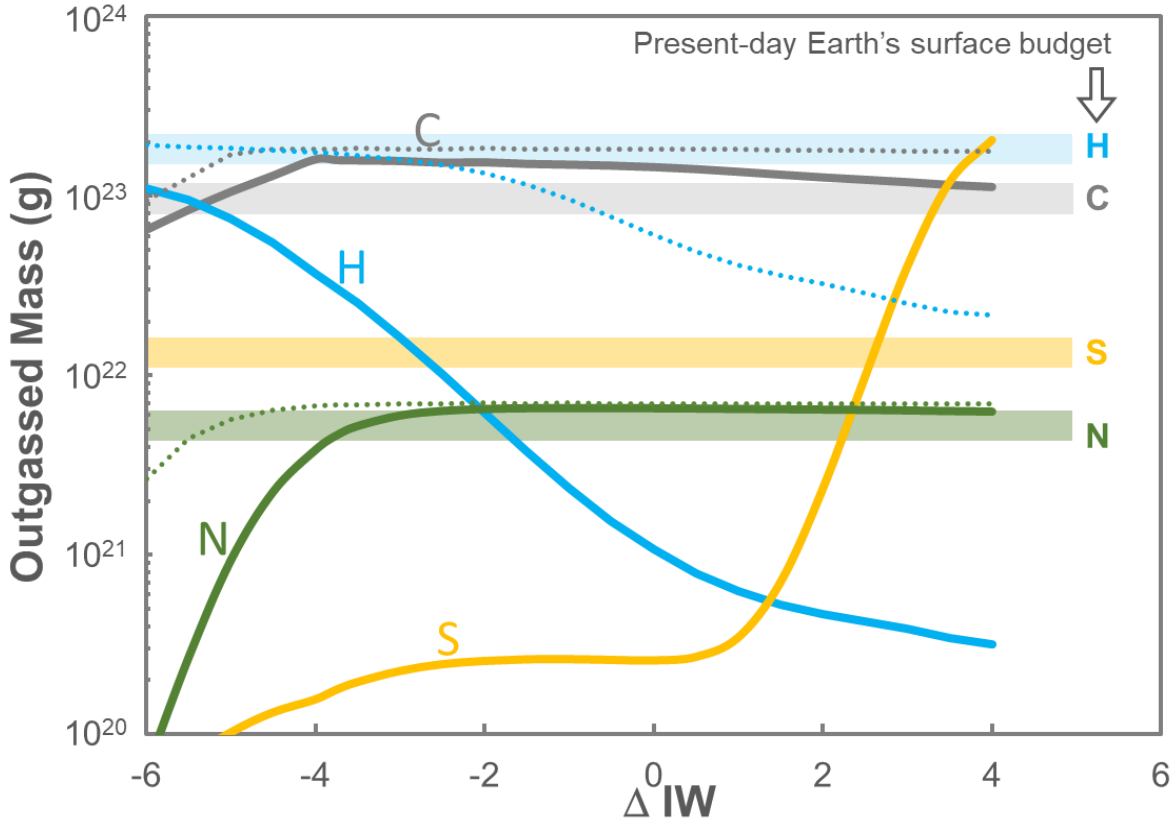

Figure S2. The outgassed masses of carbon, hydrogen, sulfur and nitrogen as a function of the oxygen fugacity at the MO surface. The horizontal bands show the present-day mass of C-H-N-S in the Earth's exosphere (atmosphere+ocean+crust). The C-O-H-N-S speciations corresponding to the outgassed masses are shown in Figure 2. The dashed line corresponds to the mass of outgassed elements from a MO crystallized at 90% and in which, H, C and N are treated as completely incompatible elements, which is not the case for sulfur. The water content dissolved in the residual melt of the 90% solidified MO is ca. 5,000-7,000 ppm H_2O at IW>0, yielding little outgassed H (gas phase with <10% H_2O). In contrast to H, the outgassing of the most volatile elements, C and N, is weakly affected by crystallisation of the MO. Our approach here is simple since we treated CHN as incompatible elements. It is, however, likely that the crystallisation of diamond, sulphide, nitrides, carbides, alloys and hydrated silicates made these elements at least moderately compatible, enabling the formation of deep volatile reservoirs. This must consider in future developments.

Supplementary references.

Bockrath C., Ballhaus C. and Holzhied A. (2004) Stabilities of laurite RuS2 and monosulfide liquid solution at magmatic temperature. Chem. Geol. 208, 265–271.

Buchanan D.L., Nolan J. (1979) Solubility of sulfur and sulfide immiscibility in synthetic tholeiitic melts and the relevance to Bushveld-complex rocks. Can Mineral 17:483-494.

Danckwerth P. A., Hess P. C. and Rutherford M. J. (1979) The solubility of sulfur in high-TiO2 mare basalts. In Proc. 10th Lunar Planet. Sci. Conf. pp. 517–530.

780 Haughton D. R., Roeder P. L. and Skinner B. J. (1974) Solubility of sulfur in mafic magmas.
781 Econ. Geol. 69, 451–467.

782 Mungall, J. E., & Brenan, J. M. (2014). Partitioning of platinum-group elements and Au
783 between sulfide liquid and basalt and the origins of mantle-crust fractionation of the chalcophile
784 elements. Geochimica et Cosmochimica Acta, 125, 265-289.

785 Nash, W., Smythe, D., Wood, B.J. (2019). Compositional and temperature effects on sulfur
786 speciation and solubility in silicate melts. Earth and Planetary Science Letters. 507. 187-198.
787 10.1016/j.epsl.2018.12.006.

788 O'Neill, H. St., Mavrogenes, J.A. (2002). The sulfide capacity and the sulfur content at sulfide
789 saturation of silicate melts at 1400 C and 1 bar. J. Petrol. 43, 1049–1087.

790 Zajacz Z., Candela P. A., Piccoli P. M., Sanchez-Valle C. and Walle M. (2013) Solubility and
791 partitioning behavior of Au, Cu, Ag and reduced S in magmas. Geochim. Cosmochim. Acta
792 112, 288–304.

793 Yoshioka, T., Nakashima, D., Nakamura, T., Shcheka, S., Keppler, H. Carbon solubility in
794 silicate melts in equilibrium with a CO-CO2 gas phase and graphite. *Geochimica et*
795 *Cosmochimica Acta* **259**, 129-143 (2019)

796

797

798

799